CrossMark

Microhardness Distribution and Microstructural Evolution in Pure Aluminum Subjected to Severe Plastic Deformation: Elliptical Cross-Sectioned Spiral Equal-Channel Extrusion (ECSEE)

Jinghui Li, Fuguo Li, Xinkai Ma, Han Chen, Zhanchao Ma, and Jiang Li

Elliptical cross-sectioned spiral equal-channel extrusion (ECSEE), one of the severe plastic deformation techniques, is of great efficiency in producing bulk ultrafine or nanostructured materials. In this paper, the simulation and experimental researches on ECSEE of high-purity aluminum were conducted to investigate the equivalent strain distribution and microhardness distribution on three orthogonal planes, as well as microstructural evolution. Simulation result shows a significant strain gradient on three planes. Microhardness tests comprise the similar results to strain distribution. According to transmission electron microscopy (TEM) results, microstructural evolution ranged from coarse structures to ultrafine structures by undergoing the shear bands, subgrains, high-angle misorientation grain boundaries and equiaxed structures. There are also some distinctions with reference to grain refinement level, grain boundary styles and dislocation distribution on different positions. The TEM investigations are in good agreement with microhardness tests.

1. Introduction

Recently, attention has been directed towards the development of new and different severe plastic deformation (SPD) techniques that may be used to fabricate ultrafine-grained materials with grain sizes in the submicrometer and the nanometer range (Ref 1-4). These techniques include equal-channel angular pressing (ECAP) (Ref 5-8), high-pressure torsion (HPT) (Ref 3, 9, 10), torsion-extrusion (TE) (Ref 11-14), combined tension-torsion (CTT) (Ref 15, 16) and elliptical cross-sectioned spiral equal-channel extrusion (ECSEE) (Ref 17-21). All of these procedures are capable of introducing large plastic straining and significant microstructural refinement in bulk crystalline solids.

It has been shown over the last two decades that a unique set of physical and mechanical properties of nanostructured materials originates mainly from two reasons: (i) size effects and (ii) the presence of high-density interfaces in the material interior (Ref 22). However, an earned grain size and nanostructure depend on the utilized SPD methods, processing

regimes, typical chemical composition, and initial microstructure of a material (Ref 7). For processing regimes, Mishra et al. (Ref 23) studied the microstructural evolution and mechanical response of copper subjected to ECAP under different processing routes, and found that the structure evolved from elongated dislocation cells (DCs) to subgrains and equiaxed grains with a diameter of ~200-500 nm. Orlov et al. (Ref 11, 24, 25) investigated the microstructural evolution of high-purity Al at the room temperature using TE. The results showed that subgrains after first TE pass owned a size of ~1.6 μm and the size remained basically the same regardless of an increase in TE passes. Haghdadi et al. (Ref 26) utilized the microhardness measurements to study the effect of pass numbers and deformation routes on hardness of commercially pure aluminum during accumulative roll bonding (ABE) processing. Wang's works (Ref 18-20) showed that severe plastic torsion straining could usually produce ultrafine-grained structure with a mean grain size of 200-300 nm.

As one of the novel SPD methods, ECSEE can achieve a heavy simple shear plastic deformation by combining extrusion-torsion deformation and be capable of producing fully dense samples with an ultrafined grain size. The principle of ECSEE process is shown in Fig. 1, where shear strain accumulates within the workpiece without changing the cross-sectional area.

Wang (Ref 18, 20) has investigated the grain refinement process of pure copper subjected to shear strain during ECSEE. However, other materials received little further attention either in microstructural evolution or in mechanical properties using the technology. Therefore, this study conducts an in-depth investigation for the microhardness distribution and microstructural evolution of pure Al during ECSEE. Pure Al is chosen for this study because the results of pure Al are well documented for other SPD processes such as ECAP, HPT, and TE.

Jinghui Li, Fuguo Li, Xinkai Ma, Han Chen, Zhanchao Ma, and **Jiang Li,** State Key Laboratory of Solidification Processing, School of Materials Science and Engineering, Northwestern Polytechnical University, Xi'an 710072, China. Contact e-mail: fuguolx@nwpu. edu.cn.
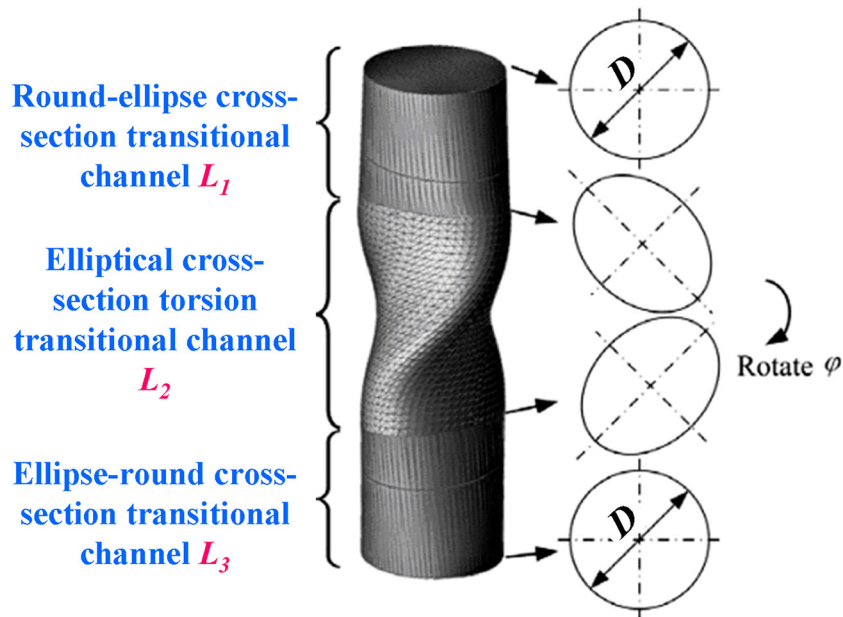
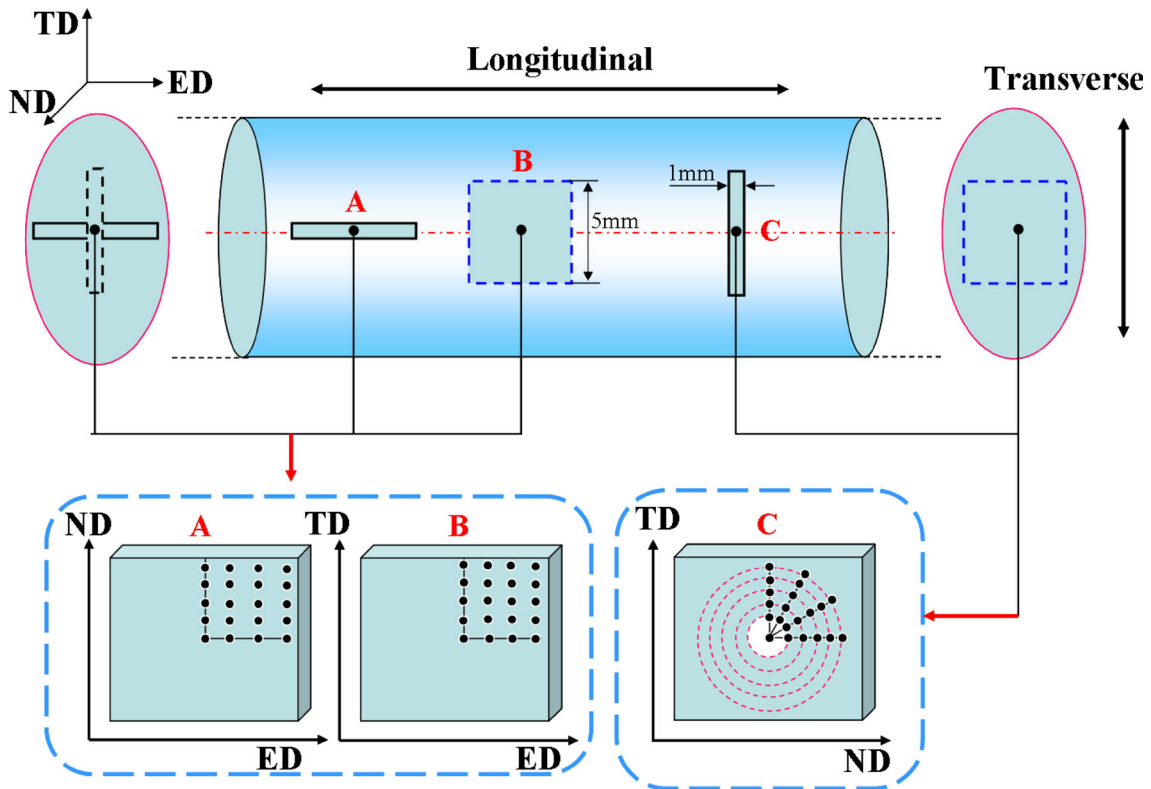**Fig. 1** Schematic diagram of the principle of ECSEE (Ref 20)

Fig. 2 Schematic illustration of candidate positions for Vickers microhardness (HV) tests

2. Simulation and Experiment

Cylindrical specimens with 10 mm in diameter and 25 mm in length were machined from the as-received 99.99%-purity aluminum billets produced by ingot casting. They were annealed at 553 K for 2 h and then cooled down at a rate of 298 K/h in order to introduce fairly homogeneous and equiaxed

microstructures. The average grain size is about 120 μm, as measured by the linear intercept method.

The ECSEE tests were carried out on the YA32-315 hydraulic press with the extrusion speed of 5 mm/min at 25 °C with lard lubrication (Ref 18). The extrusion die was a set as follows: $D_1 = 10$ mm, $L_1 = 7$ mm, $L_2 = 10$ mm, $L_3 = 7$ mm, $\phi = 120°$, and $m = 1.55$ (m was the ratio of

major-axis length to minor-axis length of the elliptical cross section) (Ref 21). The ECSEE die was made of H13 steel with a hardness of 55 RC, and a backpressure was applied to the billets by the ejector pins. With reference to the structural shape and geometry, equivalent strain of ~1 was introduced for a single pass (Ref 21). This ECSEE process was repeated up to six passes, coming to a total average strain of ~6.0. This level of strain was selected because an UFG structure was attained by ECAP (Ref 27-32) and HPT (Ref 3).
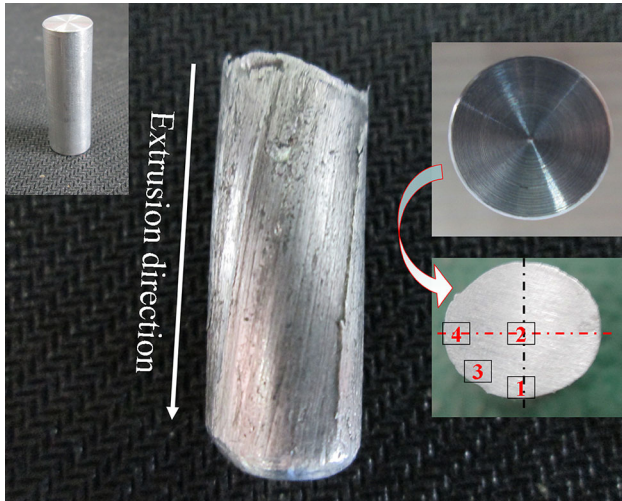

Fig. 3 TEM candidate positions of pure aluminum after ECSEE

Since the cross-sectional shape of ECSEE-ed samples was elliptical rather than round, we defined three orthogonal directions: extrusion direction (ED) parallel to the longitudinal axis, normal direction (ND) parallel to the short axes, and transverse direction (TD) parallel to long axes. Figure 2 shows the representative positions for Vickers microhardness (HV) tests using an Akashi MVK-E3 testing machine under a 100-g load applied for 15 s (Ref 33). Hardness measurements were made with an interval of 1 mm to avoid any interfering effect of adjacent indentations.

The schematic diagram of the representative locations for TEM observation of ECSEE-ed samples is shown in Fig. 3. Microstructural observation is conducted by means of a Philips Tecnai-20 transmission electron microscope with an accelerating voltage of 200 kV, the specimens for TEM analysis were well prepared with a twin-jet polisher, and a solution of 66% methanol and 33% nitric acid was used for etching.

3. Results

3.1 Equivalent Strain Distribution

Finite element simulations were used to predict the billet deformation in the different passes separately. Figure 4 shows the equivalent strain distribution on the selected positions of specimens after different passes ECSEE. After six-pass deformation, the strain value at the edge is about six, which agrees well with the analytic solution according to the Ref 21. Strain
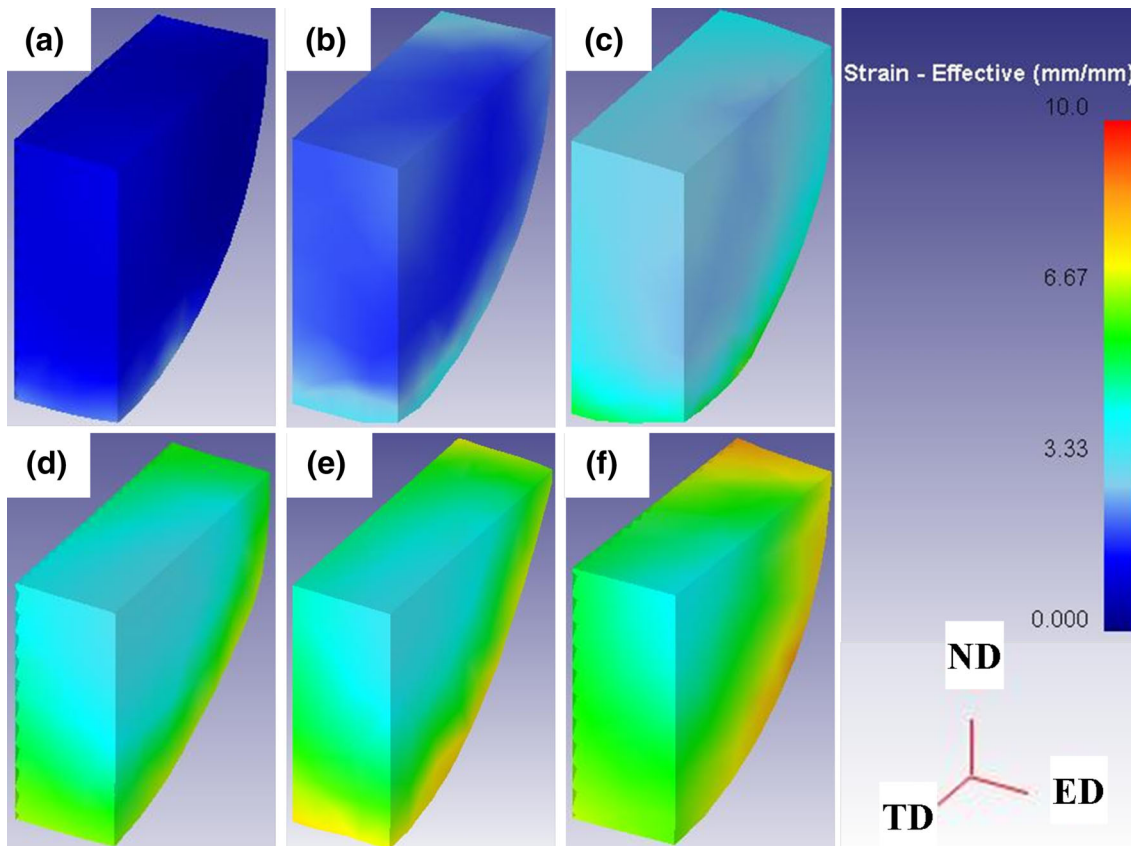

Fig. 4 Strain distribution on the selected positions of specimens after (a) 1-pass, (b) 2-pass, (c) 3-pass, (d) 4-pass, (e) 5-pass, (f) 6-pass
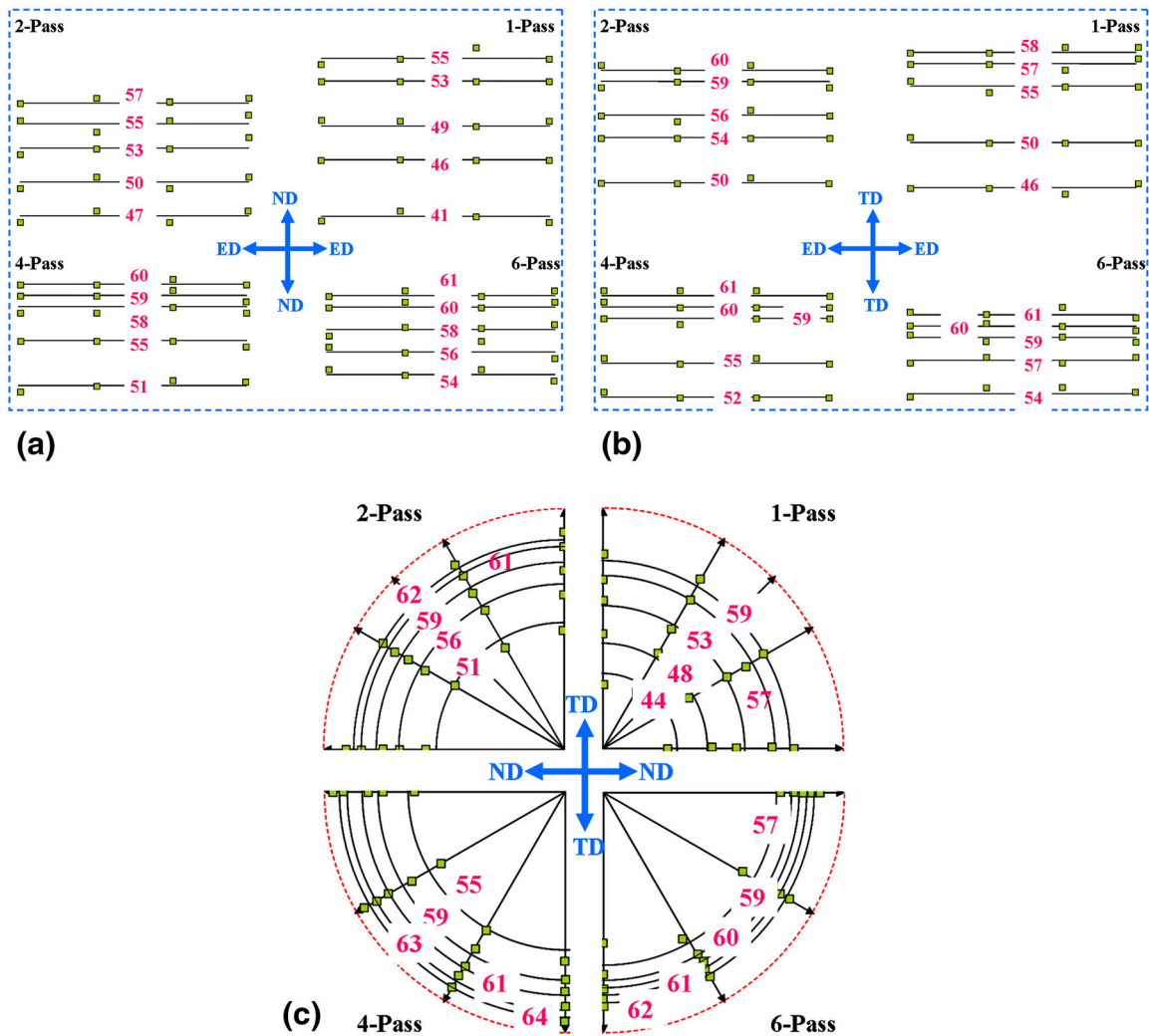
Fig. 5 Microhardness distribution on the selected positions: (a) A (ND-ED), (b) B (TD-ED), (c) C (TD-ND)

distribution on three planes is not uniform, decreasing from the edge to center. However, strain gradient gradually decreases with an increase in deformation passes, behaving as indicated by the gradually expanding green color areas seen in Fig. 4(d) to (f). The strain gradient is introduced by the torsion force during ECSEE. Similar strain gradient is more significant for HPT.

In contrast, the distribution characteristics are slightly different among these three planes. ND-ED plane owns the minimum strain gradient while TD-ND plane does the maximal one, and TD-ED plane possesses the in-between one. The differences are due to nonsymmetric deformation during ECSEE. Besides, the cross section of sample after deformation is not strictly rounded considering the volume loss and deformation damage in simulation settings.

3.2 Microhardness Distribution

Based on the correlation between the hardness and the internal deformation, hardness measurement acts as a simple and expedient procedure for reaching conclusions on the deformation characteristics and the degree of internal homogeneity within the processed work-pieces (Ref 14).

Variations of HV taken from positions A, B, and C after different ECSEE cycles are shown in Fig. 5, where green points represent the measured data. The initial microhardness on the A, B, and C planes before ECSEE is 27 HV. There is a significant increase in hardness after ECSEE; for example, after 1 pass of ECSEE (Fig. 5(a)), the Vickers hardness increases to almost twice that of initial microhardness. However, the differences between adjacent extrusion cycles become smaller, predicting the hardness saturation on TD-ND. It is important to note that the hardness values in the ND-ED and TD-ED planes are slightly lower than in the TD-ND plane. Vickers hardness in the post-processed material is inhomogeneously distributed within both the transversal and longitudinal sections, as it is minimal (41 HV) in the vicinity of the billet axis and maximal at the edge areas (55 HV) in Fig. 5(a). Similarly, inhomogeneity can be found on the TD-ED and TD-ND planes. However, the hardness gradient reduces from the central to edge areas with the increasing number of ECSEE cycles; for example, the smaller discrepancies for 6-pass ECSEE billets in comparison with other pass deformation, which illustrates that a more uniform plastic deformation could be realized by the increasing number of ECSEE cycles. This phenomenon is consistent with the
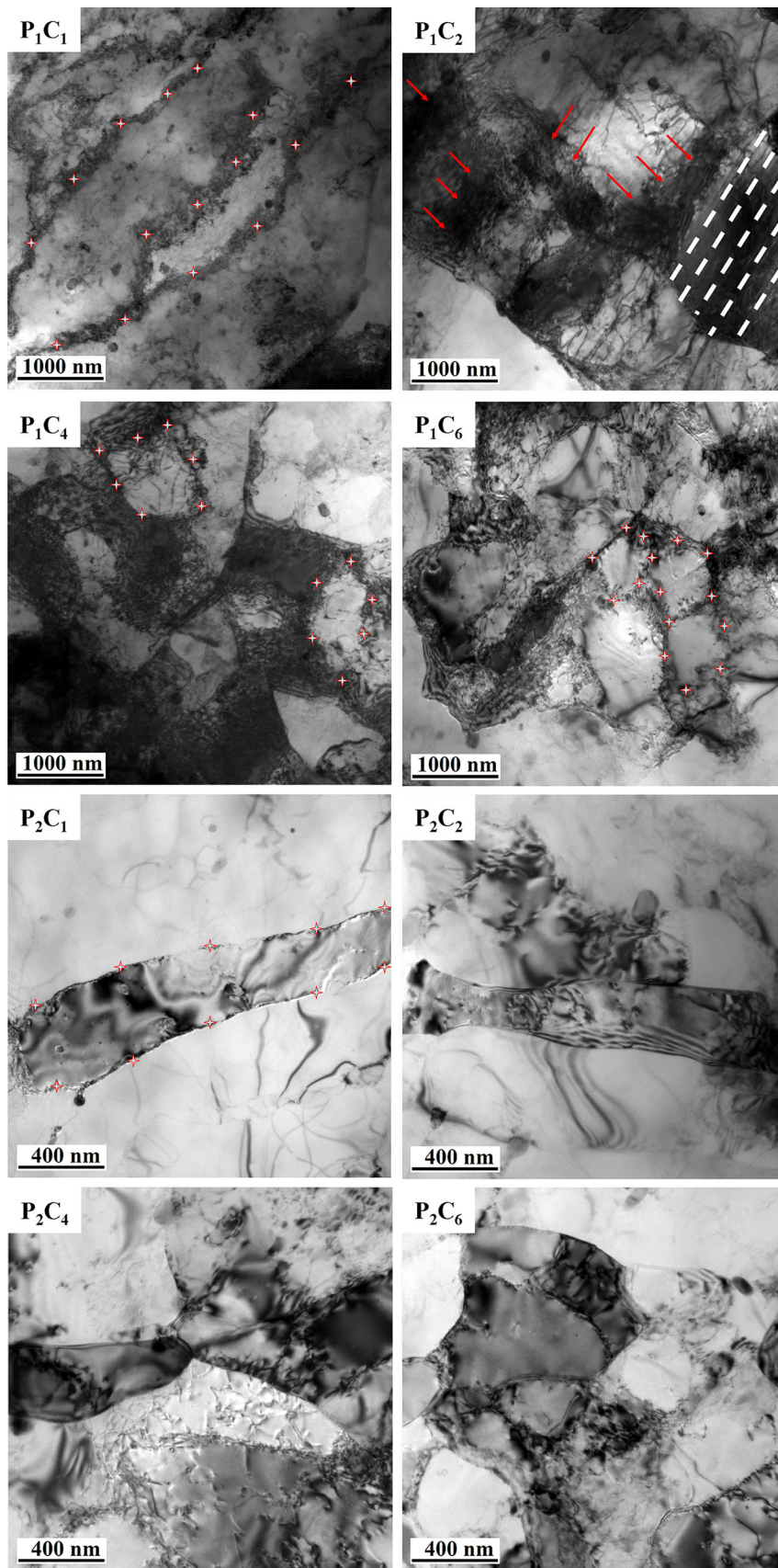
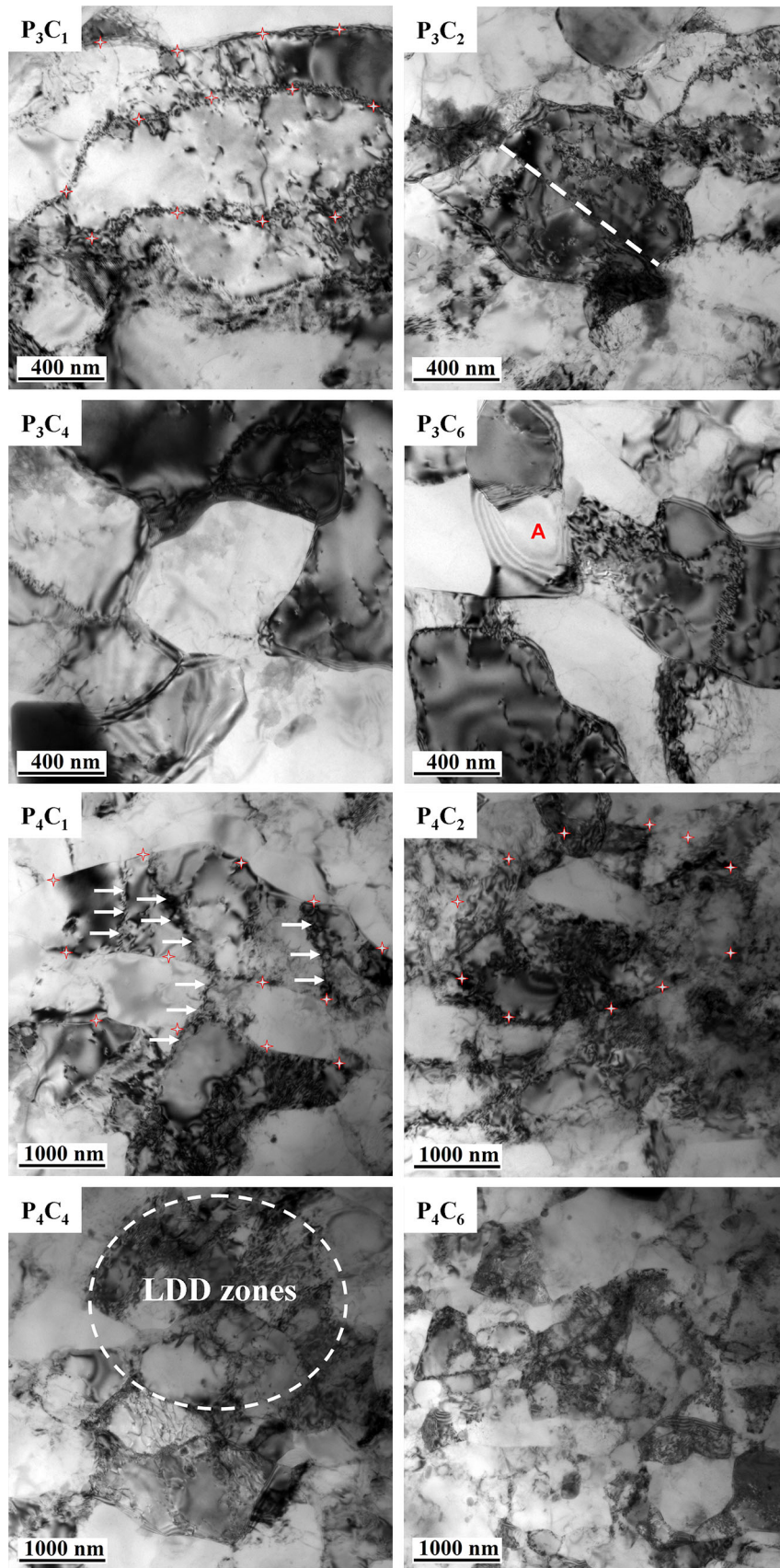**Fig. 6** TEM micrographs of candidate positions after different ECSEE passes

Fig. 6 continued

simulated strain distribution. This tendency is the same for all the planes. Kim et al. (Ref 34) have divided the pressed work-pieces into three zones (front, steady, and end zones), where a lesser shear deformation zone occurred at the outer part of the work-piece due to the faster flow of the outer part in comparison with the inner part within the main deformation zone.

3.3 Microstructural Evolution

Figure 6 shows typical TEM images of the candidate positions (Fig. 3) subjected to different ECSEE cycles, where P and C represent candidate positions and extrusion cycles, respectively. For example, P_mC_n represents that the position m is subjected to n-cycle ECSEE deformation. For P_1C_1, the original grains are clearly elongated to form shear bands (SBs) with the width of 0.5-1.2 μm as denoted by red stars. When 2-pass deformation is imposed on P_1 during ECSEE, namely P_1C_2, SBs are separated by dislocation into a large number of subgrains (SGs) or DCs, expressed by red arrows, in which a higher density of dislocations exist on the cells walls but lower density in the cell. Most of the dislocations organize dislocation walls and networks, while some are isolated. The SGs are also surrounded by a higher density of dislocations, but the dislocation density in the grain-subgrain structural elements is rather lower. On the other hand, only one single slip system is activated in some inner grains (P_1C_2), described by white dotted lines, which suggests that these larger grains undergo a low level of deformation. For 4-cycle deformation, the cell structures become much denser in the direction of extrusion. It should be noted that the GBs in P_1C_6 also have configurations of typical nonequilibrium GBs with a grain size of ∼0.4 μm.

Similar to position 1, position 2 undergoes the similar refinement process from SBs or DCs to eventually equiaxed grains with equilibrium GBs. However, some evident differences from position 1 are summarized. First, a lower level of grain refinement exists in position 2; for example, the initial SB with the width of ∼0.4 μm is retained after the second-cycle deformation (P_2C_1 and P_2C_2). Second, dislocation density is reduced compared to P_1C_4; for example, only small numbers of SBs and DCs can be found in P_2C_4.

An evident distinction between P_2C_1 and P_1C_1 is that P_2C_1 has one single SB with a sharp, straight, and narrow grain boundary. Mishra (Ref 27) has maintained the SB is completely free from dislocations. The subsequent refined SGs or DCs are surrounded by dislocations within grains (P_2C_4 and P_2C_6). Another typical feature is the extinction contours existing in the interior of the grains on position 2, which is attributed to the presence of internal stresses (Ref 35).

Apart from some general features such as GBs, SBs, and DCs during deformation, position 3 possesses several distinctions from positions 1 and 2. In terms of P_3C_1, initial coarse grain is broken into two grains, and the GBs are curved with the anchoring of dislocation. The curved boundaries and the tilt GBs images contain one single central light band and two adjacent dark broadened bands (P_3C_1). This observation is very similar to the results reported in Ref 36. Different from the curved grain boundary of P_3C_1, P_3C_2 possesses straight and narrow grain boundaries described by white dotted line, which is believed to be in an equilibrium state and are high-angle grain boundaries (HAGBs), formed by continuous dynamic recovery under large strain (Ref 37). P_3C_4 has a smooth grain boundary that is caused by the coordinated movement of adjacent grains. However, these adjacent grains situate in

different elastic stress fields characterized by the strong spreading of thickness extinction contours near the nonequilibrium boundaries. Therefore, it can be easily found that the refined SGs from P_3C_4 are subjected to uniform elastic stresses. Inspection of P_3C_6 reveals that there is a grain with a low density of dislocations as marked "A" while other grains contain many dislocations.

Position 4 has the heaviest refinement due to its position on ellipse major axis direction subjected to the heaviest straining. Different from the dislocation morphologies in the above three positions, dislocations motion is more violent in the long strip band. Dislocations pile as dislocation walls to cause the transverse brittle fracture of GBs. Besides, shrinking behavior, referred by white arrows, occurs in some shear zones due to its irregular geometry inducing the stress concentration (P_4C_1). With further deformation, dislocations are inclined to gather on grain boundaries to cause grain boundaries becoming severely bended and fuzzy (P_4C_2). The elliptical dislocation edges, surrounded by white stars shapes, may be attributed to the elliptical structure in the die cavity that promotes local grains to produce the corresponding flow. On the contrary, grains from P_4C_4 and P_4C_6 consist of the low dislocation density (LDD) zones compared to those from P_4C_2. Eventually, the grains after six cycles are made up of the grain-subgrain, nonequiaxed, and equiaxed structures, varying in size from 0.2 to 0.5 μm (P_4C_6).

4. Conclusions

(1) Strain distribution is not uniform, decreasing from the edge to center on the orthogonal planes, and the strain gradient gradually decreases with the increase in deformation passes. Vickers hardness distribution is similar to the strain distribution. Besides, the hardness values in the ND-ED and TD-ED planes are slightly lower than those in the TD-ND plane. The saturated hardness and more uniform hardness distribution can be achieved by increasing extrusion cycles.

(2) According to TEM observations, a grain refinement process is proposed for coarse microstructure broken into an ultrafine-grained structure undergoing the formation of the SBs, subgrains, high-angle misorientation grain boundaries, and equiaxed structures. However, different positions own different degrees of grain refinement, grain boundary styles, and dislocation morphology. TEM investigations are in good agreement with the microhardness test results.

Based on the significant improvement in hardness and the reduction in the grain size, ECSEE as one of the SPD techniques has a bright prospect in the future in producing bulk ultrafine or nanostructured materials.

References

1. R.Z. Valiev, R.K. Islamgaliev, and I.V. Alexandrov, Bulk Nanostructured Materials from Severe Plastic Deformation, *Prog. Mater. Sci.*, 2000, **45**(2), p 103–189

2. M.A. Meyers, A. Mishra, and D.J. Benson, Mechanical Properties of Nanocrystalline Materials, *Prog. Mater. Sci.*, 2006, **51**(4), p 427–556

3. Q. Wei et al., Microstructure and Mechanical Properties of Super-Strong Nanocrystalline Tungsten Processed by High-Pressure Torsion, *Acta Mater.*, 2006, **54**(15), p 4079–4089

4. Y. Estrin and A. Vinogradov, Extreme Grain Refinement by Severe Plastic Deformation: A Wealth of Challenging Science, *Acta Mater.*, 2013, **61**(3), p 782–817

5. V. Segal, Equal Channel Angular Extrusion: from Macromechanics to Structure Formation, *Mater. Sci. Eng. A*, 1999, **271**(1), p 322–333

6. C. Xu et al., The Evolution of Homogeneity and Grain Refinement During Equal-Channel Angular Pressing: A Model for Grain Refinement in ECAP, *Mater. Sci. Eng. A*, 2005, **398**(1), p 66–76

7. R.Z. Valiev and T.G. Langdon, Principles of Equal-Channel Angular Pressing as a Processing Tool for Grain Refinement, *Prog. Mater. Sci.*, 2006, **51**(7), p 881–981

8. R.Z. Valiev, A.P. Zhilyaev, and T.G. Langdon, Description of Severe Plastic Deformation (SPD), *Bulk Nanostructured Materials: Fundamentals and Applications*, Wiley, Hoboken, 2014, p 6–21

9. C. Xu, Z. Horita, and T.G. Langdon, The Evolution of Homogeneity in an Aluminum Alloy Processed Using High-Pressure Torsion, *Acta Mater.*, 2008, **56**(18), p 5168–5176

10. G. Sha et al., Strength, Grain Refinement and Solute Nanostructures Of an Al-Mg-Si Alloy (AA6060) Processed by High-Pressure Torsion, *Acta Mater.*, 2014, **63**, p 169–179

11. D. Orlov et al., Evolution of Microstructure and Hardness in Pure Al by Twist Extrusion, *Mater. Trans.*, 2008, **49**(1), p 2–6

12. A. Deschamps et al., Precipitation Kinetics in a Severely Plastically Deformed 7075 Aluminium Alloy, *Acta Mater.*, 2014, **66**, p 105–117

13. Y. Beygelzimer et al., Useful Properties of Twist Extrusion, *Mater. Sci. Eng. A*, 2009, **503**(1), p 14–17

14. D. Orlov et al., Plastic Flow, Structure and Mechanical Properties in Pure Al Deformed by Twist Extrusion, *Mater. Sci. Eng. A*, 2009, **519**(1), p 105–111

15. J. Li et al., Micro-structural Evolution Subjected to Combined Tension-Torsion Deformation for Pure Copper, *Mater. Sci. Eng. A*, 2014, **610**, p 181–187

16. C. Wang et al., Experimental Microindentation of Pure Copper Subjected to Severe Plastic Deformation by Combined Tension-Torsion, *Mater. Sci. Eng. A*, 2013, **571**, p 95–102

17. W. Chengpeng et al., Optimization of Structural Parameters for Elliptical Cross-Section Spiral Equal-Channel Extrusion Dies Based on Grey Theory, *Chin. J. Aeronaut.*, 2013, **26**(1), p 209–216

18. C. Wang et al., Numerical and Experimental Studies of Pure Copper Processed by a New Severe Plastic Deformation Method, *Mater. Sci. Eng. A*, 2012, **548**, p 19–26

19. C. Wang et al., Review on Modified and Novel Techniques of Severe Plastic Deformation, *Sci. China Technol. Sci.*, 2012, **55**(9), p 2377–2390

20. C. Wang et al., A Novel Severe Plastic Deformation Method for Fabricating Ultrafine Grained Pure Copper, *Mater. Des.*, 2013, **43**, p 492–498

21. C. Wang et al., Deformation Analysis of Elliptical Cross-Section Spiral Equal Channel Extrusion Technique, *Rare Met. Mater. Eng.*, 2013, **42**(4), p 679–683

22. A.E. Romanov and A.L. Kolesnikova, Application of Disclination Concept to Solid Structures, *Prog. Mater. Sci.*, 2009, **54**(6), p 740–769

23. A. Mishra et al., Microstructural Evolution in Copper Subjected to Severe Plastic Deformation: Experiments and Analysis, *Acta Mater.*, 2007, **55**(1), p 13–28

24. D. Orlov et al., Microstructure Evolution in Pure Al Processed with Twist Extrusion, *Mater. Trans.*, 2009, **50**(1), p 96

25. D. Orlov et al., Texture Evolution in Pure Aluminum Subjected to Monotonous and Reversal Straining in High-Pressure Torsion, *Scr. Mater.*, 2009, **60**(10), p 893–896

26. N. Haghdadi et al., An Investigation into the Homogeneity of Microstructure, Strain Pattern and Hardness of Pure Aluminum Processed by Accumulative Back Extrusion, *Mater. Sci. Eng. A*, 2014, **595**, p 179–187

27. A. Mishra et al., Microstructural Evolution in Copper Processed by Severe Plastic Deformation, *Mater. Sci. Eng. A*, 2005, **410**, p 290–298

28. Z. Pan et al., Microstructural Evolution and Mechanical Properties of Niobium Processed by Equal Channel Angular Extrusion up to 24 Passes, *Acta Mater.*, 2012, **60**(5), p 2310–2323

29. T. Sakai, H. Miura, and X. Yang, Ultrafine Grain Formation in Face Centered Cubic Metals During Severe Plastic Deformation, *Mater. Sci. Eng. A*, 2009, **499**(1), p 2–6

30. Y. Iwahashi et al., The Process of Grain Refinement in Equal-Channel Angular Pressing, *Acta Mater.*, 1998, **46**(9), p 3317–3331

31. S. Terhune et al., An Investigation of Microstructure and Grain-Boundary Evolution During ECA Pressing of Pure Aluminum, *Metall. Mater. Trans. A*, 2002, **33**(7), p 2173–2184

32. Z.J. Horita et al., Grain Refinement of High-Purity FCC Metals Using Equal-Channel Angular Pressing, *Mater. Sci. Forum*, 2007, **558**, p 1273–1278 (Trans Tech Publ)

33. W.J. Kim and Y.K. Sa, Micro-extrusion of ECAP Processed Magnesium Alloy for Production of High Strength Magnesium Micro-gears, *Scr. Mater.*, 2006, **54**(7), p 1391–1395

34. H.S. Kim et al., Process Modelling of Equal Channel Angular Pressing for Ultrafine Grained Materials, *Mater. Trans.*, 2004, **45**(7), p 2172–2176

35. A.A. Mazilkin et al., Softening of Nanostructured Al-Zn and Al-Mg Alloys After Severe Plastic Deformation, *Acta Mater.*, 2006, **54**(15), p 3933–3939

36. M. Liu et al., Deformation Structures in 6082 Aluminium Alloy After Severe Plastic Deformation by Equal-Channel Angular Pressing, *Mater. Sci. Eng. A*, 2008, **483**, p 59–63

37. P.B. Prangnell et al., Continuous Recrystallisation of Lamellar Deformation Structures Produced by Severe Deformation, *Acta Mater.*, 2004, **52**(11), p 3193–3206